From the Midwestern Vascular Surgical Society

Computational analysis of renal artery flow characteristics by modeling aortoplasty and aortic bypass interventions for abdominal aortic coarctation

Christopher Tossas-Betancourt, MSc,[a] Theodorus M. J. van Bakel, MD,[b] Christopher J. Arthurs, DPhil,[c] Dawn M. Coleman, MD,[b] Jonathan L. Eliason, MD,[b] C. Alberto Figueroa, PhD,[a,b] and James C. Stanley, MD,[b] *Ann Arbor, Mich; and London, United Kingdom*

ABSTRACT

Objective: Suprarenal abdominal aortic coarctation (SAAC) alters flow and pressure patterns to the kidneys and is often associated with severe angiotensin-mediated hypertension refractory to drug therapy. SAAC is most often treated by a thoracoabdominal bypass (TAB) or patch aortoplasty (PA). It is currently unclear what effect these interventions have on renal flow and pressure waveforms. This study, using retrospective data from a patient with SAAC subjected to a TAB, undertook computational modeling to analyze aortorenal blood flow preoperatively as well as postoperatively after a variety of TAB and PA interventions.

Methods: Patient-specific anatomic models were constructed from preoperative computed tomography angiograms of a 9-year-old child with an isolated SAAC. Fluid-structure interaction (FSI) simulations of hemodynamics were performed to analyze preoperative renal flow and pressure waveforms. A parametric study was then performed to examine the hemodynamic impact of different bypass diameters and patch oversizing.

Results: Preoperative FSI results documented diastole-dominated renal perfusion with considerable high-frequency disturbances in blood flow and pressure. The postoperative TAB right and left kidney volumes increased by 58% and 79%, respectively, reflecting the increased renal artery blood flows calculated by the FSI analysis. Postoperative increases in systolic flow accompanied decreases in high-frequency disturbances, aortic pressure, and collateral flow after all surgical interventions. In general, lesser degrees of high-frequency disturbances followed PA interventions. High-frequency disturbances were eliminated with the 0% PA in contrast to the 30% and 50% PA oversizing and TAB interventions, in which these flow disturbances remained.

Conclusions: Both TAB and PA dramatically improved renal artery flow and pressure waveforms, although disturbed renal waveforms remained in many of the surgical scenarios. Importantly, only the 0% PA oversizing scenario eliminated all high-frequency disturbances, resulting in nearly normal aortorenal blood flow. The study also establishes the relevance of patient-specific computational modeling in planning interventions for the midaortic syndrome. (J Vasc Surg 2019;■:1-12.)

Clinical Relevance: We performed computational fluid dynamics modeling to assess aortorenal blood flow in a child with a suprarenal abdominal aortic coarctation and to test the performance of different surgical interventions. We discovered high-frequency disturbances in the renal arteries that could potentially trigger excessive renin release. Thoracoabdominal bypass and patch aortoplasty with oversizing did not remove these disturbances completely. This could explain why the hypertension cure rates of surgical repair of suprarenal abdominal aortic coarctation are suboptimal. In addition, this study establishes the relevance of computational fluid dynamics modeling as a valuable tool to analyze complex hemodynamics and to test the performance of different surgical interventions.

Keywords: CFD; High-frequency disturbances; Optimal surgical repair; Patient-specific modeling

Fig 1. Preoperative (*left*) and postoperative (*right*) image data and corresponding computational models.

ARTICLE HIGHLIGHTS

- **Type of Research:** Retrospective case study
- **Key Findings:** Suprarenal abdominal aortic coarctation was associated with high-frequency flow disturbances in the renal arteries that could trigger increased renin release in the kidneys, leading to secondary hypertension. In general, surgical repair reduced but did not eliminate these disturbances.
- **Take Home Message:** High-frequency flow disturbances in the renal arteries could explain the limited hypertension success rates of surgical repair for suprarenal abdominal aortic coarctation. Patient-specific computational modeling offers a valuable tool to analyze complex hemodynamics in vascular disease and to test the hemodynamic performance of different surgical interventions.

Suprarenal abdominal aortic coarctations (SAACs) are often associated with renal arterial stenoses and severe renin-mediated arterial hypertension.[1] In these circumstances, the increased blood pressure and development of collateral vessels circumventing the aortic and renal artery narrowings tend to increase mean renal blood flow toward normal. However, this response is inadequate, and the abnormal release of renin persists. Whether the principal cause of the abnormal renin release is due to decreased renal artery pressure or abnormal renal artery flow waveforms is an unsettled issue.

The abnormal renin release and angiotensin generation coupled with secondary increases in aldosterone production make this form of hypertension refractory to most drug therapies. Lowering the systemic arterial pressure with drugs without treating the aortic and renal artery narrowings only results in further diminutions of intrarenal blood flow and continued excesses in renin production. Because of these medical failures, restoration of normal renal blood flow by open operative or endovascular interventions has evolved as the favored means of managing this disease.

The University of Michigan's history of treating occlusive lesions of the renal arteries and abdominal aorta in pediatric patients has extended for more than four decades.[1-6] Postoperative blood pressure control in this experience has been optimal in treating patients with isolated renal artery stenoses in contrast to less salutary outcomes when the renal artery procedures have been accompanied by a thoracoabdominal bypass (TAB) or patch aortoplasty (PA) for a coexisting abdominal aortic coarctation. Even after successful anatomic aortic and renal artery reconstructions, postoperative hypertension has been noted to persist.[1,7,8]

It is hypothesized that the aortic reconstructive procedures may not normalize renal artery blood flow. A TAB from above the SAAC to below the renal arteries may cause turbulent and abnormal renal artery perfusion as retrograde aortic flow encounters antegrade flow in the region of the renal vasculature. In addition, performance of a PA, given the commonplace practice of oversizing the patch in younger patients to accommodate later growth, may also result in abnormal renal blood flow and contribute to the persistence of the hypertensive state.

METHODS

Aortorenal blood flow was retrospectively studied using patient-specific fluid-structure interaction (FSI) simulations in a child who was treated for SAAC. Subsequently, the impact of the most commonly undertaken surgical repairs (TAB and PA) on aortorenal blood flow was analyzed. The study was approved by the University of Michigan Board of Review (HUM00112350 and HUM00006223).

Patient's history. A 9-year-old girl was referred to the authors' institution with a diagnosis of middle aortic syndrome and renin-mediated hypertension. Her initial elevated blood pressures in the range of 130 to 150/90 to 95 mm Hg were only modestly improved to the range of 140/80 mm Hg after treatment with a beta blocker and calcium channel blocker. In addition, she initially complained of lower extremity weakness and fatigue that was progressive with activity. Duplex Doppler ultrasound estimated a pressure gradient of 58 mm Hg across the SAAC. She was considered an appropriate candidate for surgical repair of the abdominal aortic coarctation.

Imaging data. Preoperative anatomy and hemodynamic data were obtained using duplex Doppler ultrasound, computed tomography angiography (CTA), and phase-contrast magnetic resonance imaging (PC-MRI). CTA imaging revealed an SAAC of 15 mm in length, with a 2.5-mm anterior-posterior diameter, and no renal artery involvement (Fig 1). The celiac artery (CA) and superior
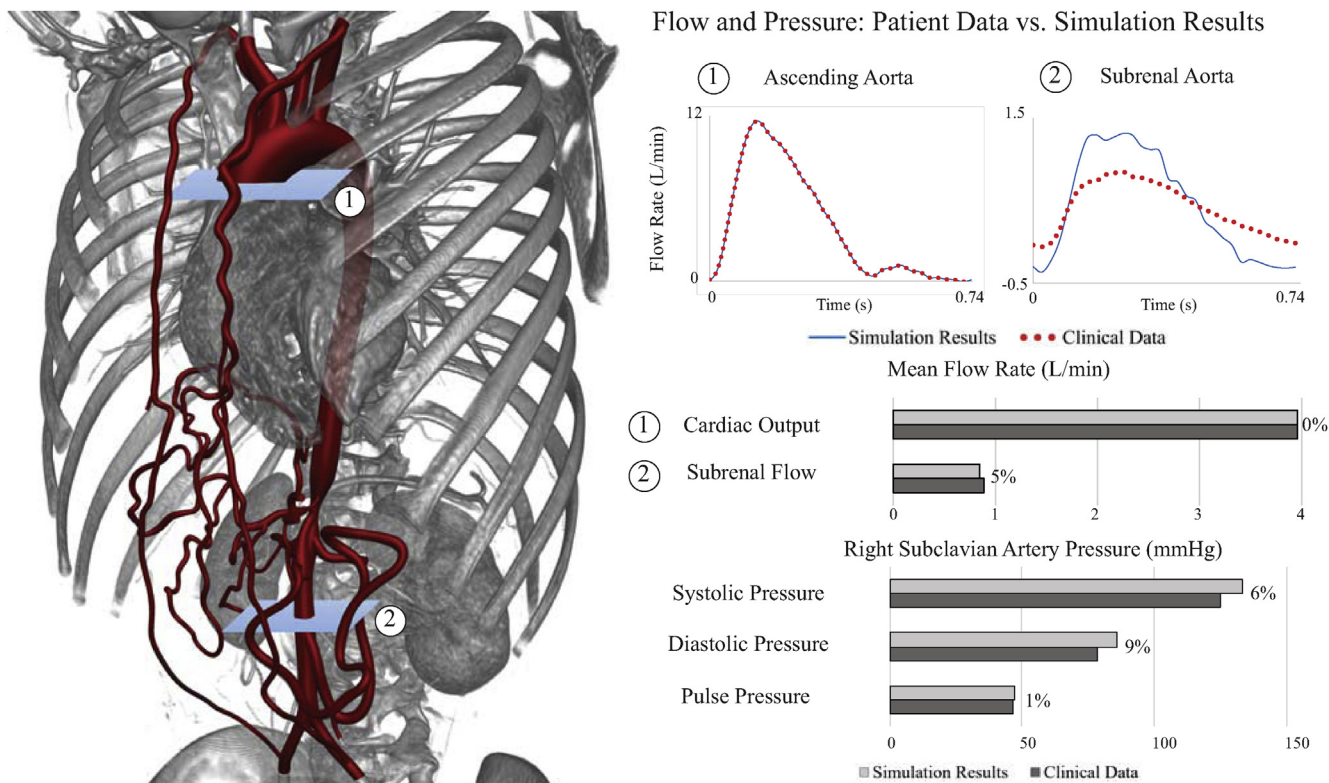
Fig 2. *Left,* Preoperative anatomy containing the phase-contrast magnetic resonance imaging (PC-MRI) planes (*1* and *2*) at which the flow measurements were acquired. *Right,* Comparison between the clinically measured flow and pressure data and the simulation results in the validated preoperative model. The clinically measured flow data (*red dotted line*) and simulated flow results (*blue line*) correspond to the indicated PC-MRI planes (*1* and *2*). The *bar graphs* compare mean values of clinical data (*dark gray*) and simulation results (*light gray*). All mean preoperative clinical flow data are matched within a 5% error margin and the pressure clinical data within a 10% error margin.

mesenteric artery (SMA) arose from the coarctation itself, and both exhibited ostial narrowings. Extensive collaterals circumvented the coarcted aorta, with an intact inferior mesenteric artery being the dominant source of blood flow to the intestines. The internal mammary arteries were enlarged and communicated with the epigastric arteries that had multiple collaterals to the lower extremities and abdominal visceral organs. MRI examinations performed at 10 days and 1 year after the TAB provided postoperative data for analysis.

TAB. The basis for choosing a TAB over a PA was that the 2.5-mm diameter of the coarctation and the involvement of the CA and SMA would have made an aortoplasty inordinately challenging and risky. In this case, a midline abdominal incision was made from the xiphoid to the pubis, followed by medial visceral rotation of the left colon to provide exposure of the entire abdominal aorta.

The supraceliac aorta was occluded with a Satinsky clamp, after which a 14-mm polytetrafluoroethylene bypass graft was anastomosed to a lateral aortotomy. The proximal aorta was occluded for 17 minutes, during which time blood flow to the lower extremities and abdominal

viscera, although reduced, was maintained through the pre-existing large retroperitoneal and abdominal wall collaterals. The graft was then clamped just beyond its aortic origin, and antegrade aortic blood flow was restored after removal of the supraceliac aortic clamp. The graft was passed behind the left kidney and then anastomosed in an end-to-side manner to a lateral aortotomy just above the inferior mesenteric artery (Fig 1). During the distal anastomosis, the infrarenal aorta was occluded for a time similar to that of the proximal anastomosis.

Kidney size. Preoperative and 10-day postoperative kidney volumes were measured using semiautomatic segmentation tools in Mimics version 21.0 (Materialise NV, Leuven, Belgium).

Computational modeling. Patient-specific FSI simulations[9] were performed to assess preoperative blood flow and to compare the hemodynamic performance of TAB vs PA using a "virtual testing" paradigm.[10] First, a preoperative model was created and calibrated to match the anatomic and hemodynamic clinical data (Fig 2). Then, the calibrated preoperative model was
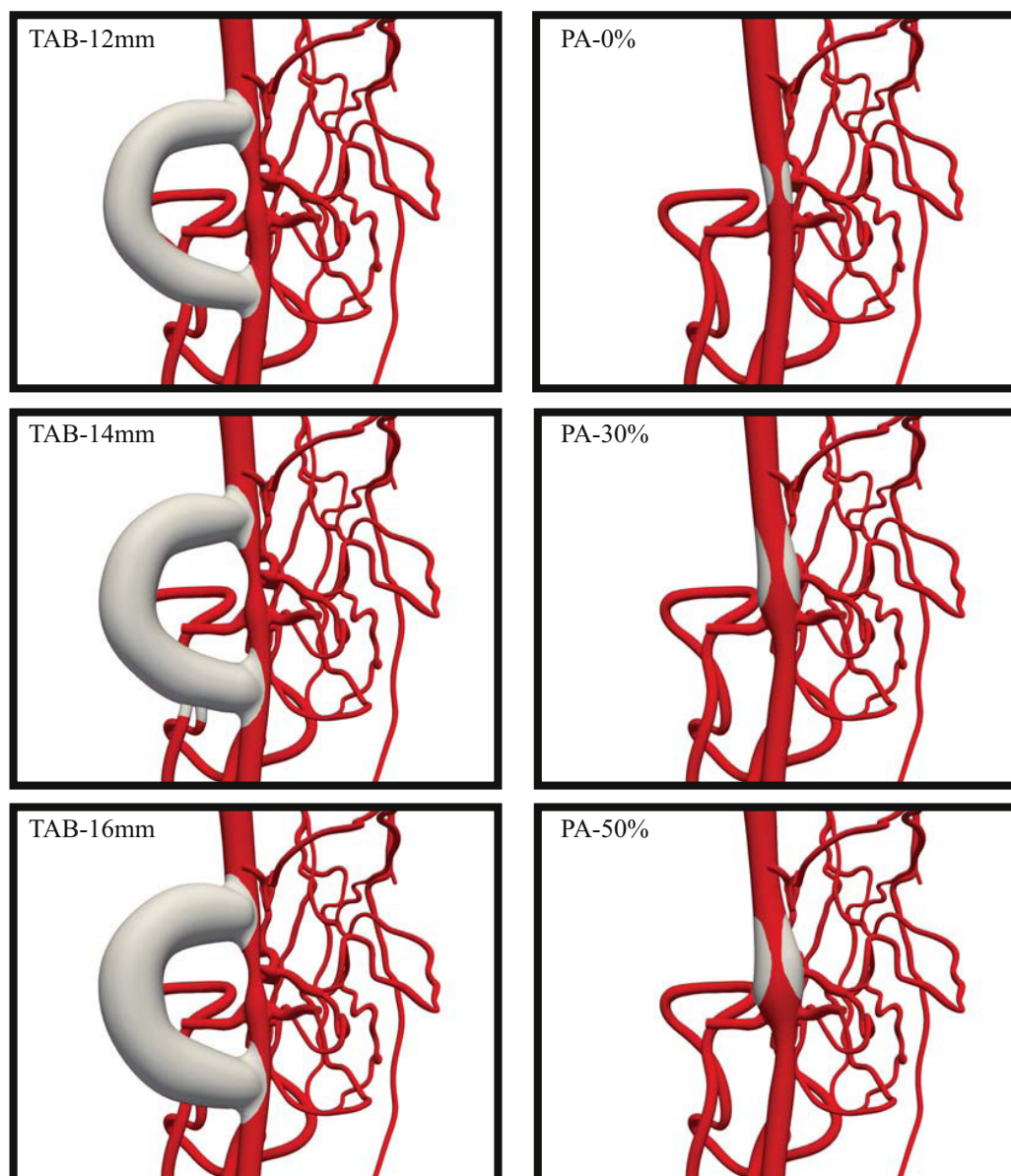
Fig 3. Close-up posterior views of the abdominal coarctation region and the renal arteries of all thoracoabdominal bypass (*TAB*; *left*) and patch aortoplasty (*PA*; *right*) surgical options. Graft material of the bypass and patch is presented in *gray*.

adapted to reflect six surgical interventions (Fig 3), including three different TABs with 12-mm, 14-mm, and 16-mm diameters, respectively (TAB-12 mm, TAB-14 mm, and TAB-16 mm), and three different PAs producing increases in aortic diameters of 0%, 30%, and 50% (PA-0%, PA-30%, and PA-50%) relative to the native aorta. In addition, a control case was constructed by adjusting the preoperative model to produce a healthy anatomy without coarctation and collateral vessels (Supplementary Fig 3, online only). All models were constructed from the CTA image data using Cardiovas-culaR Integrated Modeling and SimulatiON (CRIMSON) version 2017.07.01, developed by King's College London

(London, United Kingdom) and the University of Michigan (Ann Arbor, Michigan) under the support of the European Research Council.[11] Besides the vascular anatomy, each FSI model requires specification of arterial wall material properties (thickness and stiffness) as well as outflow boundary conditions at each branch. These boundary conditions represent the compliance and resistance of the distal vasculature not included in the anatomic model. The wall properties and outflow boundary conditions were calibrated to match the simulation results with the clinically acquired flow and pressure data and to achieve reasonable regional flow distributions (Fig 2).[12] The methods for specification of
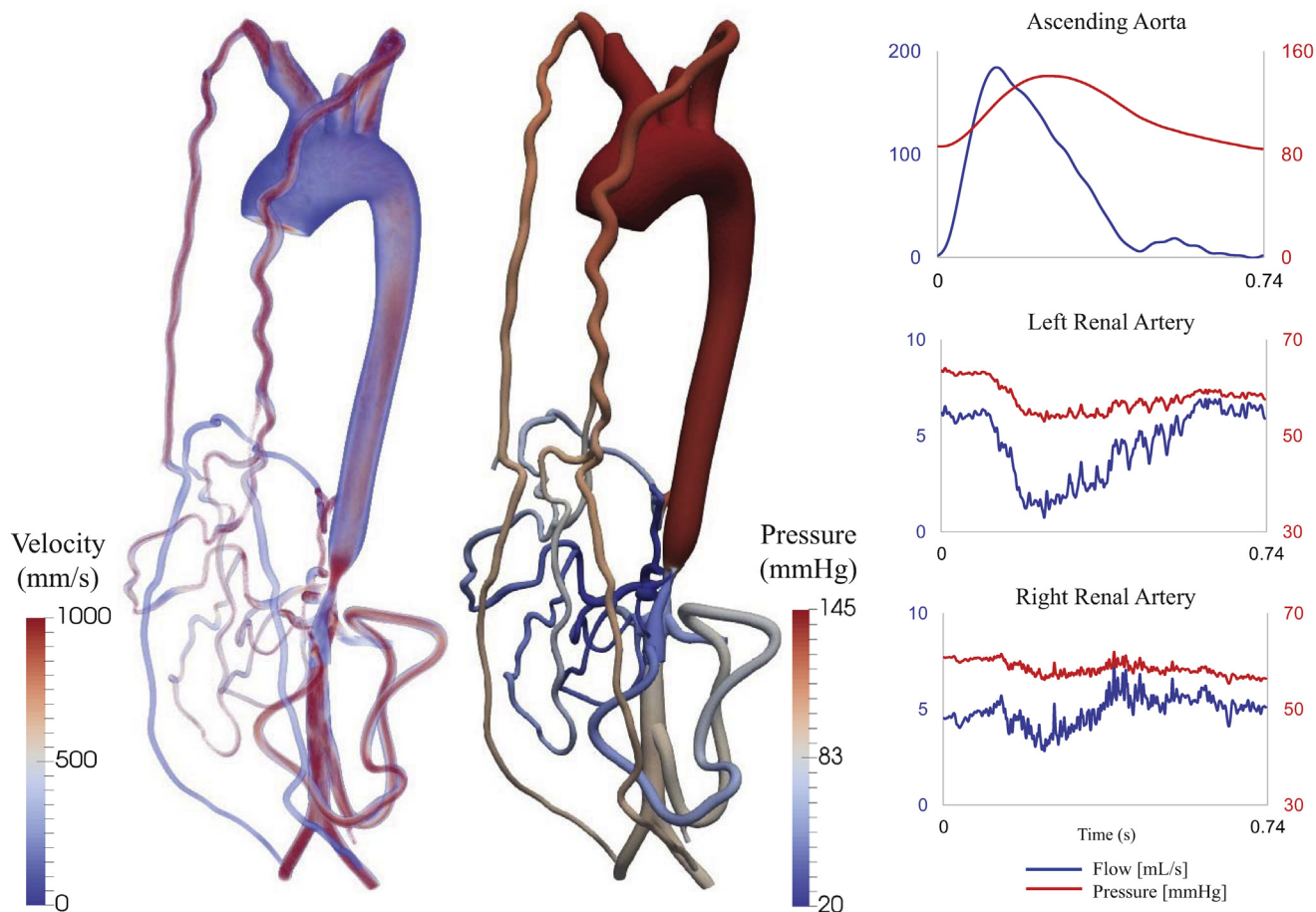
Fig 4. *Left,* Three-dimensional maps of preoperative hemodynamics in peak systole. Note the high velocities and large pressure gradient through the coarctation. *Right,* Flow (*blue*) and pressure (*red*) waveforms in the ascending aorta, left renal artery, and right renal artery. The renal artery waveforms reveal diastole-dominated flows with high-frequency disturbances and low pressures compared with aortic pressure.

the boundary conditions and material properties are reported in detail in the Appendix (online only). In the control case, the boundary conditions were tuned to match the preoperative flow splits and a blood pressure appropriate for this patient's size and age (96/65 mm Hg).[13] In the postoperative models, cardiac output and outflow boundary conditions were kept the same as preoperative conditions with the exception of the supra-aortic arteries, for which the outflow boundary conditions were adjusted to reproduce literature data on regional flow splits.[14]

Computations. Blood was modeled as an incompressible Newtonian fluid with a density of 1060 kg/m^3 and a dynamic viscosity of 4.0 Pa·s. Computations were performed using the CRIMSON Navier-Stokes flow solver on 160 cores at the University of Michigan high-performance computing cluster ConFlux. Simulations were run until cycle-to-cycle periodicity was achieved in the pressure fields; this typically took three to five cycles. Computation time per cardiac cycle was approximately 48 hours.

RESULTS

Postoperative course. Complete resolution of the patient's lower extremity discomfort was evident in the early postoperative period. Her serum creatinine concentration, which ranged from 0.48 to 0.57 mg/dL preoperatively, decreased to 0.28 to 0.3 mg/dL postoperatively. However, she remained mildly hypertensive during her postoperative hospitalization, and at 1-year follow-up she remained on a low-dose calcium channel blocker with resting blood pressures in the range of 110 to 115/65 to 70 mm Hg.

Preoperative simulation. The baseline preoperative model successfully reproduced the patient's hemodynamic data, as documented in a comparison between clinical data and simulation results at different locations in the circulation (Fig 2). The computed flows were all within 5% of the clinically measured data, and computed pressures were within 10%.

The FSI simulation results revealed a pressure gradient of 55 mm Hg across the coarctation at peak systole (Fig 4), which matched the pressure gradient derived
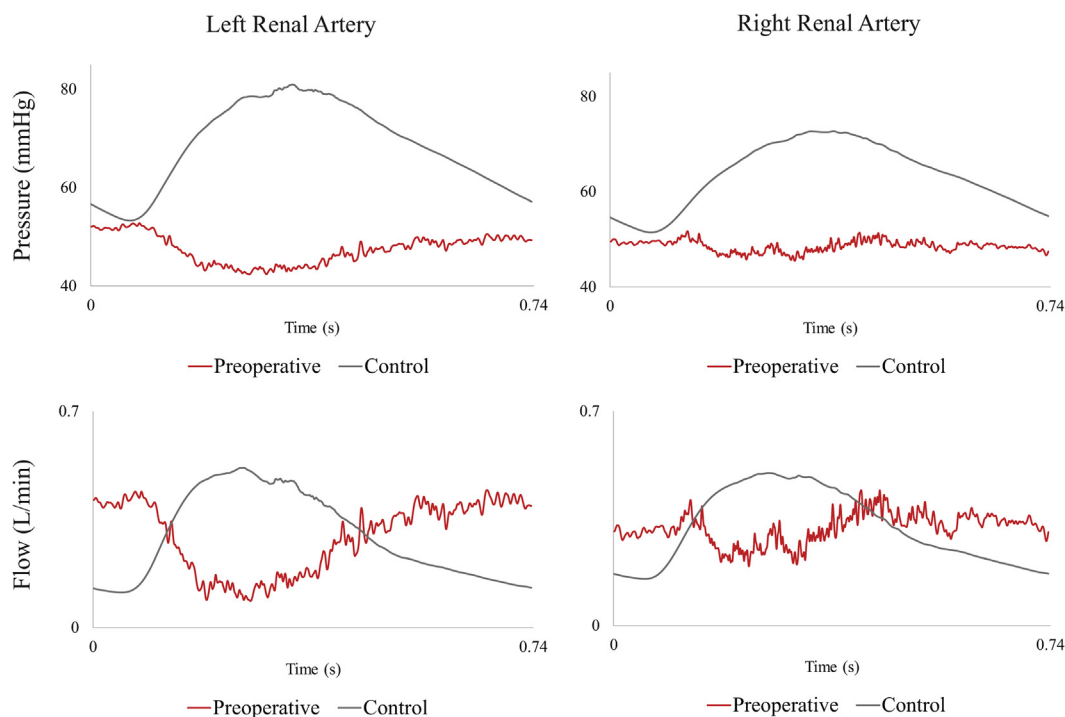
Fig 5. Comparison of the renal artery waveforms between the preoperative and control cases shows that removal of the pathologic anatomy results in higher renal pressures, elimination of the high-frequency disturbances, and systole-dominated waveforms.

from duplex Doppler ultrasound (58 mm Hg). In addition, disturbed flow patterns were present distal to the coarctation that propagated into the renal arteries. Assessment of the renal artery flow and pressure waveforms revealed diastole-dominated renal flows with high-frequency oscillations (Fig 4; Video, online only). Renal artery pressure was markedly lower than ascending aortic pressure.

In the control case, systole-dominated renal flows without high-frequency disturbances were found. The results for the control anatomy are presented in the Video (online only) and Supplementary Fig 3 (online only). A direct comparison of the pressure and flow waveforms between preoperative and control cases is reported in Fig 5.

Postoperative simulations. The computed mean flows at the outlets of the preoperative model and all six surgical repair models (Table) were revealing. All six interventions successfully reduced pressures at the ascending aorta (Fig 6) and increased renal artery flow rates (Table). Furthermore, all surgical repairs resulted in systole-dominated flow waveforms (Fig 7), with a reduction of the high-frequency flow and pressure disturbances in the renal arteries (Figs 7 and 8). Although most postoperative simulations retained some degree of the high-frequency oscillations, the PA-0% eliminated the high-frequency oscillations completely.

The flow waveforms from the TAB-14 mm simulation were compared with the PC-MRI data at 1-year follow-up

(Fig 9). The patient's cardiac output decreased during follow-up (−13%, from 3.9 to 3.2 L/min). The shape of the waveform changed as a result of a reduction in ventricular afterload following surgery. The computed (TAB-14 mm) and 1-year follow-up PC-MRI data on flow through the bypass documented an excellent match; the percentages of cardiac output through the bypass were 38% and 39% for the computations and the PC-MRI data, respectively.

Kidney size. Considerable changes in the kidney length were noted at 10-day follow-up. To accurately quantify the change in kidney size, volumetric measurements of both kidneys were obtained (Fig 10). Right and left kidney lengths increased from 3.4 cm to 3.85 cm (+13%) and from 3.8 cm to 4.6 cm (+21%), respectively. Right and left kidney volumes increased from 50.3 cm^3 to 79.6 cm^3 (+58%) and from 51.5 cm^3 to 92.0 cm^3 (+79%), respectively. The observed increments in kidney volume reflected the calculated increases in right and left renal flow from the TAB-14 mm FSI analysis (+9% and +26%, respectively).

DISCUSSION

Abdominal aortic coarctation is a rare vascular disease recognized most frequently in pediatric patients. The aortic narrowings are commonly associated with ostial stenoses of the CA, SMA, and renal arteries.[15] This is clinically referred to as the middle aortic syndrome, which is manifested in most patients with drug therapy-resistant arterial hypertension.[16]

Table. Simulated mean flow rates (mL/min)

Vessel	Preoperative model	TAB-12 mm	TAB-14 mm	TAB-16 mm	PA-0%	PA-30%	PA-50%
Left common carotid artery	275	351	319	308	321	344	356
Left subclavian artery	269	330	305	295	305	328	336
Right common carotid artery	276	351	320	309	321	344	357
Right subclavian artery	274	325	306	296	305	328	331
SMA	573	566	528	534	551	557	580
Left gastric artery	292	207	265	273	262	233	212
Splenic artery	300	175	249	257	267	227	219
Hepatic artery 1	98	50	94	101	94	80	60
Hepatic artery 2	159	84	128	124	127	108	101
Left renal artery	291	394	370	374	353	360	360
Right renal artery	313	337	345	350	331	331	317
Inferior mesenteric artery	91	84	78	79	75	74	76
Left iliac artery	278	255	230	233	226	227	230
Right iliac artery	282	262	236	239	232	231	235
Renal flow	605	732 (+21%)	715 (+18%)	724 (+20%)	684 (+13%)	691 (+14%)	677 (+12%)
Mesenteric flow	1421	1082 (−24%)	1263 (−11%)	1289 (−9%)	1301 (−8%)	1206 (−15%)	1173 (−17%)
Cerebral blood flow	551	702 (+27%)	639 (+16%)	617 (+12%)	642 (+17%)	688 (+25%)	713 (+29%)

PA, Patch aortoplasty; *SMA*, superior mesenteric artery; *TAB*, thoracoabdominal bypass.
Mean flow to the kidneys is calculated by the sum of the left and right renal arteries. Mean flow to mesenteric region includes all flow through the left gastric artery, splenic artery, hepatic artery 1, and hepatic artery 2. Mean cerebral flow includes flow in the left and right common carotid arteries. Percentages are reported relative to the preoperative model.
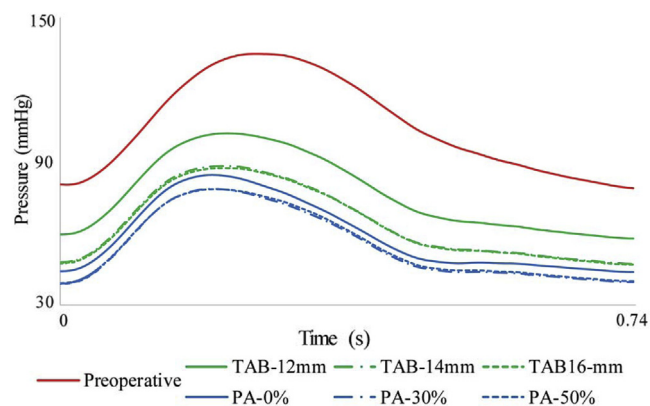
Fig 6. Ascending aortic pressure waveforms in all models. All postoperative models exhibited an important pressure reduction compared with the preoperative state. Patch aortoplasty (*PA*) procedures resulted in a greater decrease of aortic pressure compared with thoracoabdominal bypass (*TAB*) procedures.

Classic canine experiments noted that the location of the abdominal coarctation plays a key role in the presence of hypertension.[17] Hypertension is commonly observed in cases in which the coarctation is suprarenal or involves the renal arteries. Conversely, hypertension is mostly absent when the coarctation is distal to the renal arteries. An investigation by Scott and Bahnson[18] of canine hypertension due to surgically induced coarctation of the aorta that resulted in hypertension at 5 to 7 weeks noted that transposition of a kidney to a level above the coarctation and contralateral nephrectomy resulted in disappearance of hypertension. These earlier experiments suggested that disturbed aortorenal blood flow contributes to hypertension in abdominal coarctation.

In treating middle aortic syndrome, conventional surgical reconstructive procedures and catheter-based interventions are favored over long-term drug therapy.[1,7,19-22] Operative planning is usually derived solely from preoperative imaging.[23] Surgical decisions are often based on technical issues at hand, rather than aiming to restore normal aortorenal blood flow. Unfortunately, endovascular balloon dilation with or without stenting of abdominal aortic narrowings has had limited use with mixed early results and few long-term successes. Open operations, such as TAB and PA, have been the most common form of treatment of abdominal aortic coarctations. These operations often lead to improved hypertension control, yet most cases still depend on antihypertensive therapy to maintain normal blood pressures for sex and age.

Many factors go into decision-making for performing a PA vs a TAB. A PA is favored in most instances of a limited aortic coarctation distant from the CA, SMA, and renal arteries. In assessing the long-term benefits of PA in younger patients, the patch is intentionally oversized to account for the child's expected growth. Nevertheless, the appropriate degree of patch oversizing has not been established. Likewise,
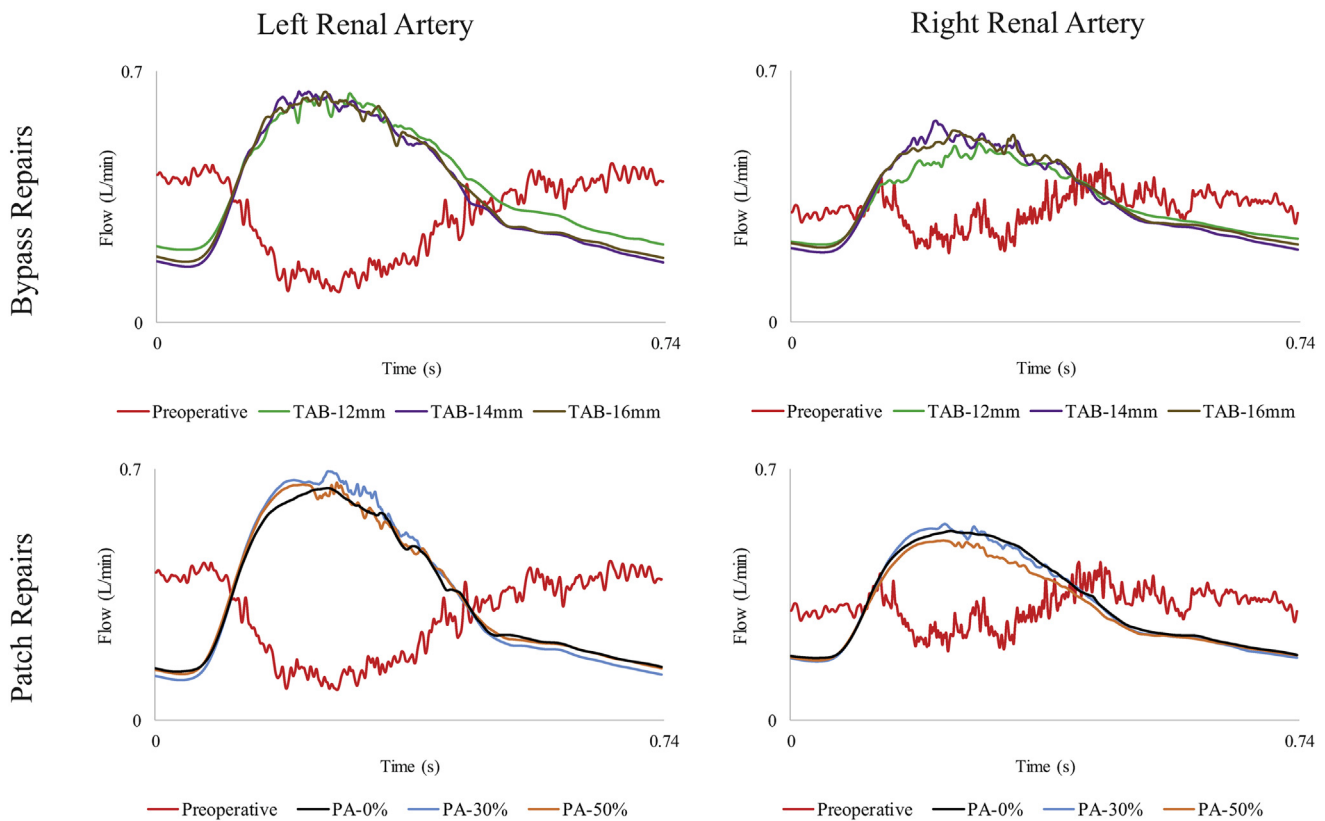
Fig 7. Renal flow waveforms in all models. Both thoracoabdominal bypass (*TAB*) and patch aortoplasty (*PA*) resulted in restoration of systole-dominated renal flows, reduction of high-frequency disturbances, and increased flow. Some degree of high-frequency disturbance persisted in all postoperative scenarios, with the exception of PA-0%, which revealed nearly normal renal flow waveforms.

the effects on renal artery blood flow accompanying a disproportionately enlarged aorta after a PA are unknown.

A TAB is the procedure of choice in treating more severe coarctations with abdominal aortic diameters of only a few millimeters. In this case, a PA would have nearly overlapping sutures from the lateral walls of the patch. In the past, the authors have recommended a wide range of TAB diameters related to age, with the intent that the bypass diameter would at least be 60% to 70% of the predicted adult aorta.[1] These recommendations may be logical, but as noted with PA oversizing, the science behind such is meager.

Clinical experience. The authors recently reviewed their experience with 155 children having renal artery stenotic disease and renovascular hypertension.[6] Hypertension outcomes were better in children treated with renal artery reconstructions alone compared with those requiring additional aortic procedures. The hypertension cure, improved, and failure rates in patients without aortic disease (n = 98) were 50%, 34%, and 16%, respectively. These outcome rates were 33%, 59%, and 8% in patients additionally treated with PA (n = 28) and 35%, 50%, and 15% in patients additionally treated with TAB (n = 29). Given the

poorer outcomes in patients undergoing concomitant aortic procedures, one must question whether abnormal aortorenal flow remains after surgery and whether differences exist in surgical repair between TAB and PA.

Computational modeling. Computational modeling is a widely used method in engineering fields that can be applied to study complex flow dynamics. Image-based computational tools have been developed for cardiovascular disease research,[24,25] medical device evaluation,[26] and, more recently, virtual planning of surgical interventions.[9] Whereas the "virtual testing" paradigm has largely replaced the traditional "build-and-test" (eg, trial and error) paradigm in other engineering fields, this is not yet the case in the medical field. As evident in this investigation, the value of computational modeling is apparent in preoperative determination of the therapeutic impact of different sizes of TAB and PA in patients with the midaortic syndrome.

Computational modeling in this investigation provided data of much higher spatial (up to 0.05 mm) and temporal (0.025 millisecond) resolution than are available in any contemporary imaging test. These high-resolution data revealed an unexpected and potentially relevant finding
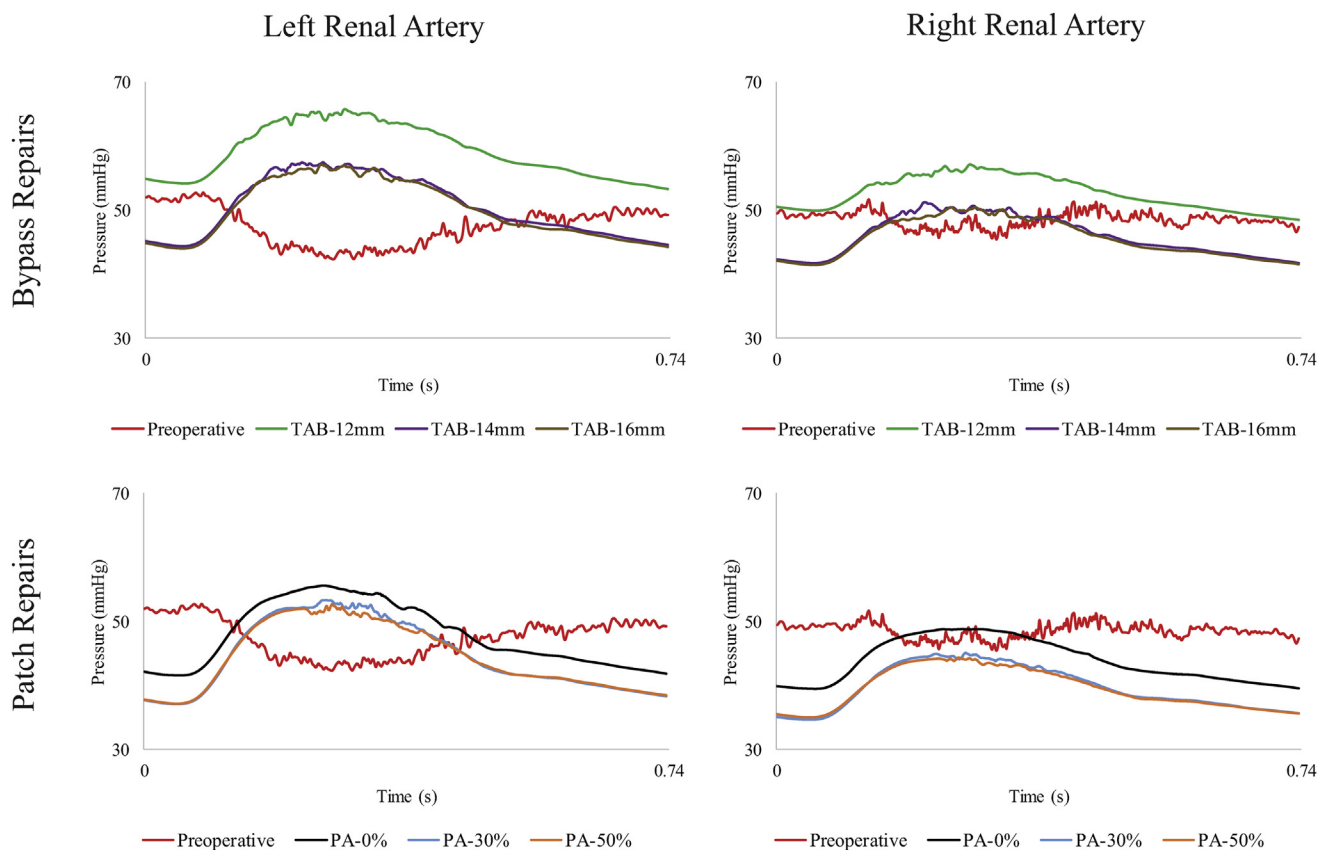
Fig 8. Renal pressure waveforms in all models. Most surgical repairs resulted in a reduction in renal artery pressures, associated with the large reductions in aortic pressures in all postoperative models (Fig 6). *PA,* Patch aortoplasty; *TAB,* thoracoabdominal bypass.

of high-frequency disturbances in the renal arteries preoperatively that could explain an increased renin release in the kidneys, resulting in secondary hypertension. Persistent high-frequency disturbances were also found in the postoperative models and might explain the continuing hypertension after both TAB and PA interventions in patients undergoing concomitant renal artery reconstructions.

Besides characterization of preoperative aortorenal blood flow, this study also analyzed the impact of different TAB diameters and degree of PA oversizing. In total, six different surgical treatment options were studied: three TAB diameters and three levels of PA oversizing. All surgical interventions resulted in reduced aortic pressures and increased renal flows with restoration of systole-dominated waveforms.

An unexpected finding of this investigation was that most surgical repairs resulted in a reduction in renal artery pressures (Fig 8). This acute response of the system, which does not account for any autoregulatory processes after surgery, is reflective of the large reductions in aortic pressures in all postoperative models (Fig 6).

Importantly, various degrees of high-frequency disturbance persisted postoperatively, the exception being the treatment with a 0% PA, which eliminated the

high-frequency disturbances completely. These results suggest that excessive PA oversizing and TAB lead to high-frequency disturbances that may contribute to continued renin-mediated hypertension.

In the TAB operations, the high-frequency disturbances could be explained by the turbulent mixing of antegrade flow through the remaining aortic stenosis and retrograde flow through the TAB. Changing the TAB graft diameter did not significantly affect the persistence of high-frequency disturbances. Such flow abnormalities could explain why the patient in this case report, who had undergone a TAB repair, was still dependent on antihypertensive medication at 1-year follow-up. In an oversized PA, the dilated segment of the reconstruction induces flow disturbances. Flow clearly shows complex recirculation and vortices in the region of the patch (Fig 11), similar to what is observed in aneurysmal disease. The absence of dilation in the PA-0% case explains the lack of disturbances in this model. Furthermore, it may also explain the reduced hypertension cure rates of renal artery revascularizations in the authors' larger series of patients requiring concomitant aortic procedures.

Historically, renin-mediated hypertension has been linked to low perfusion pressure and low renal blood
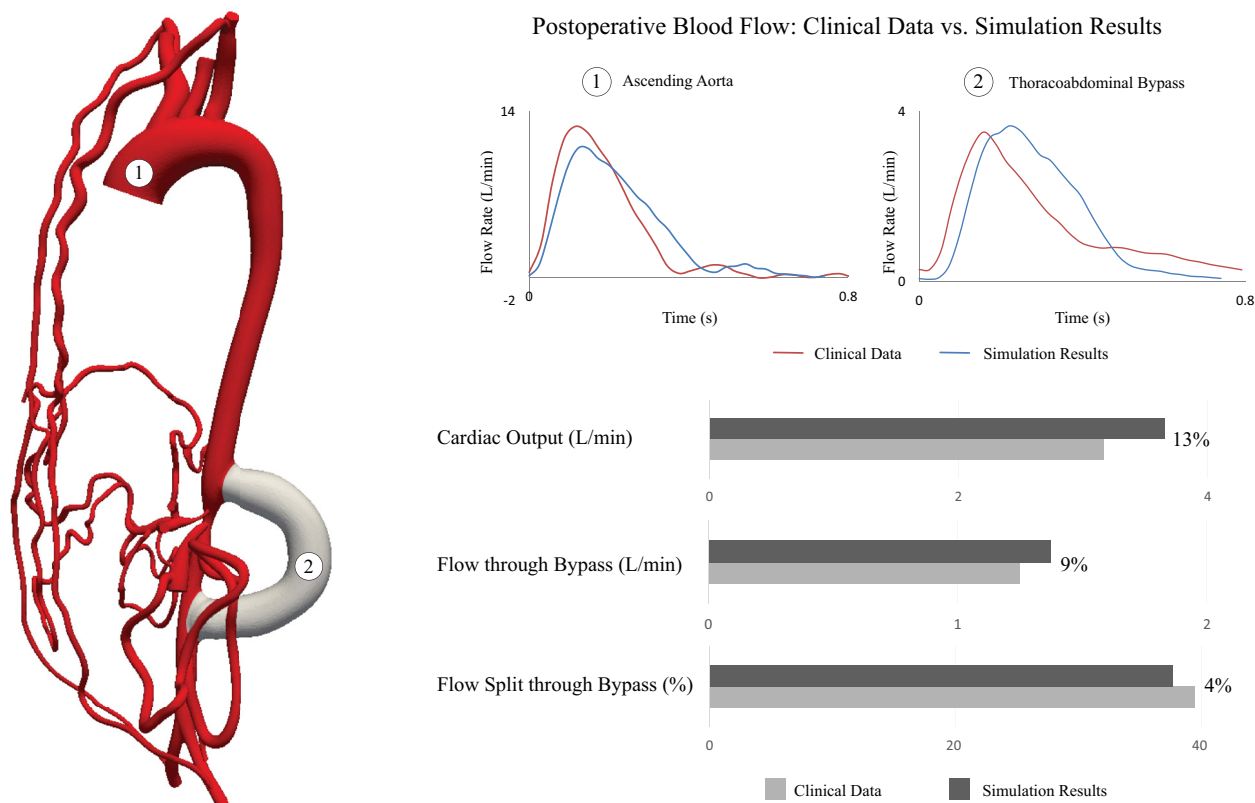
Fig 9. Comparison of the flow waveforms from the thoracoabdominal bypass (TAB) 14-mm-diameter simulation results and phase-contrast magnetic resonance imaging (PC-MRI) data at 1-year follow-up. Cardiac output decreased during follow-up (from 3.9 to 3.2 L/min). The shape of the waveform changed as a result of a reduction in ventricular afterload following surgery. The computed (TAB-14 mm) and 1-year follow-up PC-MRI data on flow through the bypass documented an excellent match; the percentages of cardiac output through the bypass were 38% and 39% for the computations and the PC-MRI data, respectively.

flow.[23] The high-frequency flow oscillations observed in this work have not been described in the earlier literature. The most likely explanation for this is that contemporary clinical measurement devices lack the temporal resolution necessary to detect such high-frequency flow oscillations. It has been recognized that Doppler ultrasound, CTA, and MRI can be helpful in the evaluation of renovascular disease, but none have, at present, high enough sensitivity to rule out renovascular disease in a child with a suggestion of that diagnosis.[27]

Limitations. The stiffness properties of the aortic wall could not be calculated with the available data in this study. Therefore, in this investigation, the assigned stiffness parameters were derived from a previous study from our laboratory that characterized aortic stiffness in a cohort of pediatric patients with aortic coarctation.[28] In that study, the aortic stiffness was calculated using strain measurements from MRI and invasive pressure measurements from catheterization.

This investigation analyzed aortorenal blood flow in a single patient with SAAC. Whereas the results for this patient were clinically validated, performing the same analysis in patients with different anatomic features might result in different outcomes, including the presence of high-frequency disturbances in the renal arteries. In addition, the causality between the high-frequency disturbances and excessive renin release should be further investigated. We tested six different surgical interventions with arbitrary TAB and PA sizes. Performing a parametric study of other patch and bypass sizes and configurations could result in different outcomes.

Furthermore, even though a specific intervention might theoretically render a better hemodynamic outcome, performance of the procedure itself may be inordinately challenging and risky, resulting in a technical failure and less successful outcome. Thus, acceptance of benefits defined by virtual testing must be tempered by clinical judgment and expertise.

Last, the results presented here do not take into account any of the vascular autoregulations that undoubtedly occur after a vascular reconstruction. The magnitude of the waveforms, specifically the pressure,
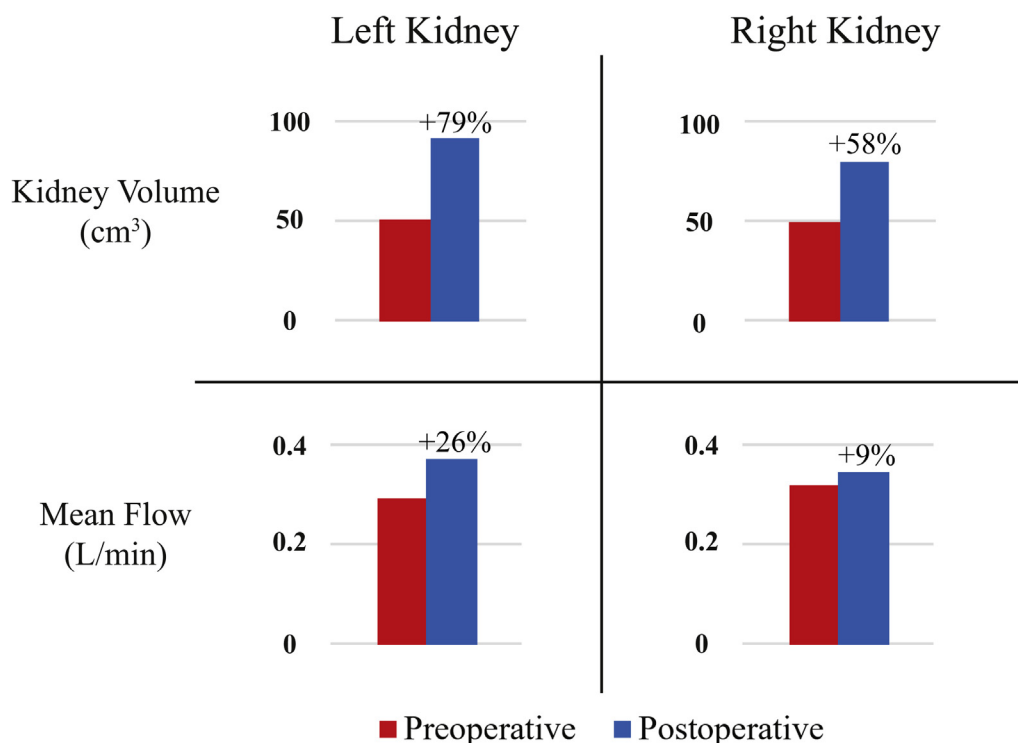
Fig 10. Preoperative (*red*) and postoperative thoracoabdominal bypass (TAB) 14-mm-diameter (*blue*) clinically measured kidney volumes and mean simulated renal artery flow rates. Percentages indicate the change from the preoperative to the postoperative conditions.
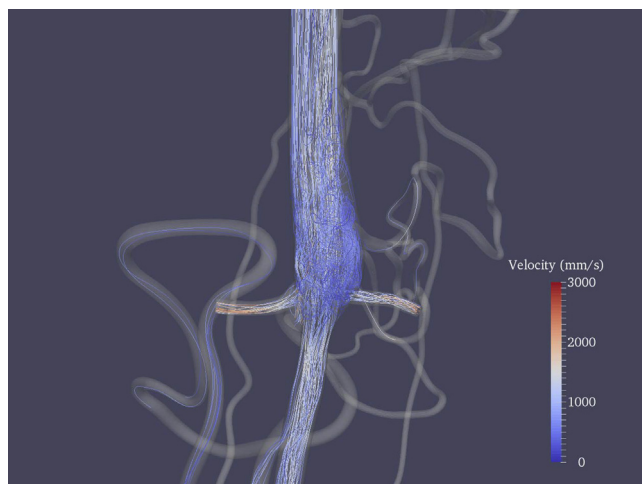
Fig 11. Velocity streamlines for the patch aortoplasty (PA)-50% model at mid-deceleration (*t* = 0.30 second). Disturbed flow patterns are clearly evident in the region of the patch, propagating into the renal arteries.

might change as a result of systemic vasoreactivity, although the high-frequency disturbances are likely to persist.

CONCLUSIONS

This study has revealed the presence of high-frequency disturbances in renal blood flow and pressure after operative interventions for SAAC. These previously unrecognized disturbances may be a fundamental contributor to continued abnormal release of renin and thus the basis of the often-seen persistent postoperative hypertension in this population of patients.

Considerable value resides in computational modeling of vascular surgery procedures. Patient-specific modeling provides high-resolution hemodynamic information for differing interventions and allows preoperative planning for complex procedures, such as those accompanying aortic reconstructions in young patients with SAAC. Collaborative efforts between biomedical engineers and clinicians will be essential to provide accurate modeling and simulation of feasible surgical procedures in this setting.

AUTHOR CONTRIBUTIONS

REFERENCES

1. Stanley JC, Criado E, Eliason JL, Upchurch GR, Berguer R, Rectenwald JE. Abdominal aortic coarctation: surgical treatment of 53 patients with a thoracoabdominal bypass, patch aortoplasty, or interposition aortoaortic graft. J Vasc Surg 2008;48:1073-82.

2. Fry WJ, Ernst CB, Stanley JC, Brink B. Renovascular hypertension in the pediatric patient. Arch Surg 1973;107: 692-8.

3. Stanley JC, Fry WJ. Pediatric renal artery occlusive disease and renovascular hypertension. Etiology, diagnosis, and operative treatment. Arch Surg 1981;116:669-76.

4. Stanley JC, Zelenock GB, Messina LM, Wakefield TW. Pediatric renovascular hypertension: a thirty-year experience of operative treatment. J Vasc Surg 1995;21:212-26; discussion: 226-7.

5. Stanley JC, Criado E, Upchurch GR, Brophy PD, Cho KJ, Rectenwald JE. Pediatric renovascular hypertension: 132 primary and 30 secondary operations in 97 children. J Vasc Surg 2006;44:1219-28.

6. Coleman DM, Eliason JL, Jackson T, Kershaw DB, Williams DM, Ganesh SK, et al. SS26 surgical management of pediatric renovascular hypertension. J Vasc Surg 2017;65:138S.

7. Rumman RK, Nickel C, Matsuda-Abedini M, Lorenzo AJ, Langlois V, Radhakrishnan S, et al. Disease beyond the arch: a systematic review of middle aortic syndrome in childhood. Am J Hypertens 2015;28:833-46.

8. Rocchini AP, Rosenthal A, Barger AC, Castaneda AR, Nadas AS. Pathogenesis of paradoxical hypertension after coarctation resection. Circulation 1976;54:382-7.

9. Figueroa CA, Vignon-Clementel IE, Jansen KE, Hughes TJ, Taylor CA. A coupled momentum method for modeling blood flow in three-dimensional deformable arteries. Comput Methods Appl Mech Eng 2006;195:5685-706.

10. van Bakel TM, Lau KD, Hirsch-Romano J, Trimarchi S, Dorfman AL, Figueroa CA. Patient-specific modeling of hemodynamics: supporting surgical planning in a Fontan circulation correction. J Cardiovasc Transl Res 2018;11: 145-55.

11. CRIMSON. The software for cardiovascular modelling and simulation. Available at: www.crimson.software. Accessed May 17, 2019.

12. Xiao N, Alastruey J, Figueroa CA. A systematic comparison between 1-D and 3-D hemodynamics in compliant arterial models. Int J Numer Method Biomed Eng 2013;30:204-31.

13. National High Blood Pressure Education Program Working Group on High Blood Pressure in Children and Adolescents. The fourth report on the diagnosis, evaluation, and treatment of high blood pressure in children and adolescents. Pediatrics 2004;114(Suppl 4th Report):555-76.

14. Lantz BM, Foerster JM, Link DP, Holcroft JW. Regional distribution of cardiac output: normal values in man determined by video dilution technique. AJR Am J Roentgenol 1981;137:903-7.

15. Cohen JR, Birnbaum E. Coarctation of the abdominal aorta. J Vasc Surg 1988;8:160-4.

16. Panayiotopoulos YP, Tyrrell MR, Koffman G, Reidy JF, Haycock GB, Taylor PR. Mid-aortic syndrome presenting in childhood. Br J Surg 1996;83:235-40.

17. Goldblatt H, Kahn JR, Hanzal RF. Studies on experimental hypertension: IX. The effect on blood pressure of constriction of the abdominal aorta above and below the site of origin of both main renal arteries. J Exp Med 1939;69:649-74.

18. Scott HW, Bahnson HT. Evidence for a renal factor in the hypertension of experimental coarctation of the aorta. Surgery 1951;30:206-17.

19. Porras D, Stein DR, Ferguson MA, Chaudry G, Alomari A, Vakili K, et al. Midaortic syndrome: 30 years of experience with medical, endovascular and surgical management. Pediatr Nephrol 2013;28:2023-33.

20. Sandmann W, Dueppers P, Pourhassan S, Voiculescu A, Klee D, Balzer KM. Early and long-term results after reconstructive surgery in 42 children and two young adults with renovascular hypertension due to fibromuscular dysplasia and middle aortic syndrome. Eur J Vasc Endovasc Surg 2014;47:509-16.

21. Sethna CB, Kaplan BS, Cahill AM, Velazquez OC, Meyers KEC. Idiopathic mid-aortic syndrome in children. Pediatr Nephrol 2008;23:1135-42.

22. Tummolo A, Marks SD, Stadermann M, Roebuck DJ, McLaren CA, Hamilton G, et al. Mid-aortic syndrome: long-term outcome of 36 children. Pediatr Nephrol 2009;24: 2225-32.

23. Castelli PK, Dillman JR, Smith EA, Vellody R, Cho K, Stanley JC. Imaging of renin-mediated hypertension in children. AJR Am J Roentgenol 2013;200:W661-72.

24. Taylor CA, Figueroa CA. Patient-specific modeling of cardiovascular mechanics. Annu Rev Biomed Eng 2009;11:109-34.

25. van Bakel TM, Arthurs CJ, Nauta FJ, Eagle KA, van Herwaarden JA, Moll FL, et al. Cardiac remodelling following thoracic endovascular aortic repair for descending aortic aneurysms. Eur J Cardiothoracic Surg 2018 Dec 6. [Epub ahead of print].

26. van Bakel TM, Arthurs CJ, van Herwaarden JA, Moll FL, Eagle KA, Patel HJ, et al. A computational analysis of different endograft designs for zone 0 aortic arch repair. Eur J Cardiothoracic Surg 2018;54:389-96.

27. Tullus K, Roebuck DJ, McLaren CA, Marks SD. Imaging in the evaluation of renovascular disease. Pediatr Nephrol 2010;25: 1049-56.

28. Sotelo JA, Valverde I, Beerbaum PB, Greil GF, Schaeffter T, Razavi R, et al. Pressure gradient prediction in aortic coarctation using a computational-fluid-dynamics model: validation against invasive pressure catheterization at rest and pharmacological stress. J Cardiovasc Magn Reson 2015;17(Suppl 1):Q78.

APPENDIX (online only).

Finite element meshes contained 2 to 4 million tetrahedral elements, and localized refinement was performed using an adaptive technique in regions of high velocities and complex flow.[1] The assigned stiffness parameters were derived from a study within our group that characterizes aortic stiffness in a cohort of pediatric patients with aortic coarctation.[2] In that study, the stiffness was measured using phase-contrast magnetic resonance imaging and invasive pressure measurements from catheterization.

The workflow consisted of initially building and validating the preoperative model. The clinically acquired measurements of preoperative cardiac output, aortic pressure, and subrenal flow were matched by tuning the parameters of Windkessel models.[3] Three-element Windkessel models were used to represent the resistance and compliance of the anatomy distal to the model's outlets.[4] The proximal resistor was set as 5% of the total resistance in all outflow branches, with the exception of the carotid, subclavian, and renal arteries, for which the relative value for the proximal resistor was increased to eliminate backflow. In addition, the inlet flow waveform was reduced by 5% to account for the flow going to the enlarged lumbar arteries that are not included in the computational models.

A mesh dependence analysis was conducted to ensure that the presence of high-frequency disturbances in the preoperative model was independent of mesh size. The renal artery flow waveforms from models containing 2.5 million elements and 4.9 million elements were compared (Supplementary Fig 1). The presence of high-frequency flow disturbances persists in the renal arteries of the model with the refined mesh (4.9 million elements). This confirms that the high-frequency disturbances are not dependent on mesh size. The results reported in this work were obtained using the mesh containing 2.5 million elements.

To analyze time step size dependency of the high-frequency disturbances in the preoperative model, an analysis was conducted whereby the time step size was decreased to one fifth of the original (Δt = 5e−6 second). The high-frequency disturbances were present in the renal flow waveforms of both simulations (Supplementary Fig 2), confirming that the presence of these disturbances is independent of the time step size.

To compare the diseased aortic hemodynamics with a "healthy" control, the model of the preoperative anatomy was modified by removing the aortic coarctation, ostial stenoses of visceral arteries, and collaterals. The model of the control healthy anatomy is presented in Supplementary Fig 3. The boundary conditions of the control case were tuned to match preoperative flow splits (Supplementary Table I) and a normal blood pressure for the patient's size and age (96/65 mm Hg).[5] The control case showed healthy hemodynamics in the ascending aorta and renal arteries. The renal artery flow and pressure waveforms (Supplementary Fig 3) show systole-dominated waveforms without high-frequency disturbances.

In the virtual repair scenarios, flow distribution to the supra-aortic arteries was severely diminished because of the removal of the effective resistance created by the coarctation. An autoparameterization scheme was applied to 5 of the 14 outlets to match proper supra-aortic flow distributions postoperatively.[6] The five outlets that underwent autoparameterization were the following: right common carotid, right subclavian artery, left common carotid, left subclavian artery, and superior mesenteric artery. After autoparameterization was performed, the simulations of all surgical interventions were run with the same outflow boundary condition parameters (Supplementary Table II).

REFERENCES

1. Sahni O, Müller J, Jansen KE, Shephard MS, Taylor CA. Efficient anisotropic adaptive discretization of the cardiovascular system. Comput Methods Appl Mech Eng 2006;195: 5634-55.
2. Sotelo JA, Valverde I, Beerbaum PB, Greil GF, Schaeffter T, Razavi R, et al. Pressure gradient prediction in aortic coarctation using a computational-fluid-dynamics model: validation against invasive pressure catheterization at rest and pharmacological stress. J Cardiovasc Magn Reson 2015;17(Suppl 1):Q78.
3. Xiao N, Alastruey J, Figueroa CA. A systematic comparison between 1-D and 3-D hemodynamics in compliant arterial models. Int J Numer Method Biomed Eng 2013;30:204-31.
4. Vignon-Clementel IE, Figueroa CA, Jansen KE, Taylor CA. Outflow boundary conditions for 3D simulations of non-periodic blood flow and pressure fields in deformable arteries. Comput Methods Biomech Biomed Engin 2010;13:625-40.
5. National High Blood Pressure Education Program Working Group on High Blood Pressure in Children and Adolescents. The fourth report on the diagnosis, evaluation, and treatment of high blood pressure in children and adolescents. Pediatrics 2004;114(Suppl 4th Report):555-76.
6. Arthurs CJ, Lau KD, Asrress KN, Redwood SR, Figueroa CA. A mathematical model of coronary blood flow control: simulation of patient-specific three-dimensional hemodynamics during exercise. Am J Physiol Hear Circ Physiol 2016;310:H1242-58.

Left Renal Artery

Right Renal Artery
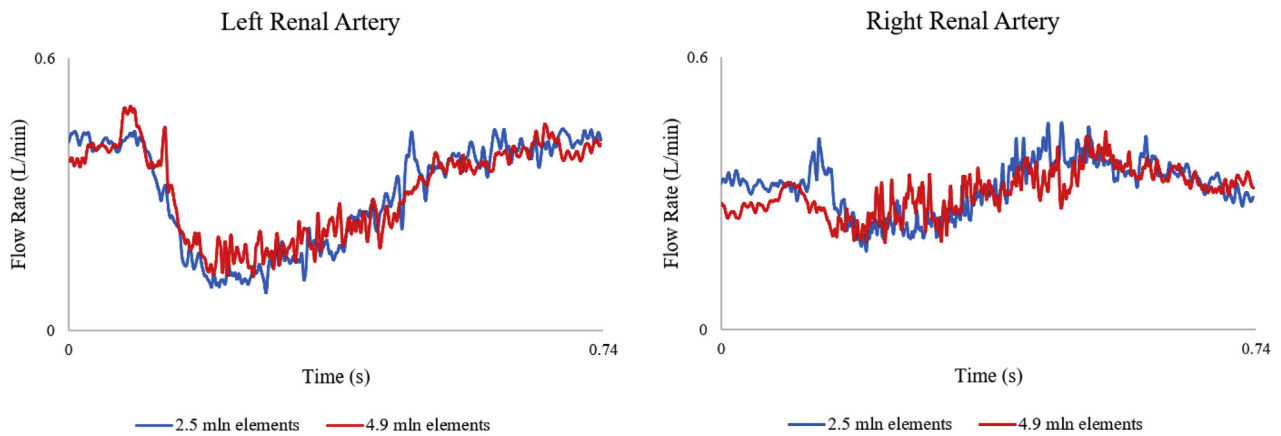
Supplementary Fig 1 (online only). Renal flow waveforms in preoperative models with mesh sizes of 2.5 million elements (*blue*) and 4.9 million elements (*red*). Local mesh refinement methods were used to increase mesh size in the region of the aortic narrowing and renal arteries.[1] The high-frequency disturbances persisted after refinement of mesh.

Left Renal Artery

Right Renal Artery
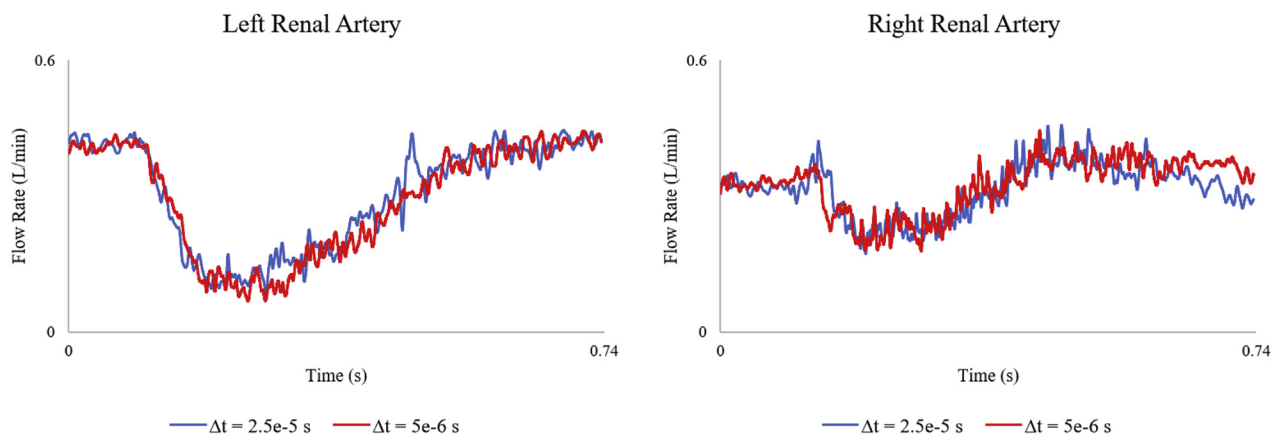
Supplementary Fig 2 (online only). Simulations of the preoperative model were run with a time step size of 2.5e−5 second (*blue*) and 5e−6 second (*red*). All waveforms exhibit high-frequency disturbances, confirming that the presence of high-frequency disturbances was independent of time step size.

Tossas-Betancourt et al   12.e3
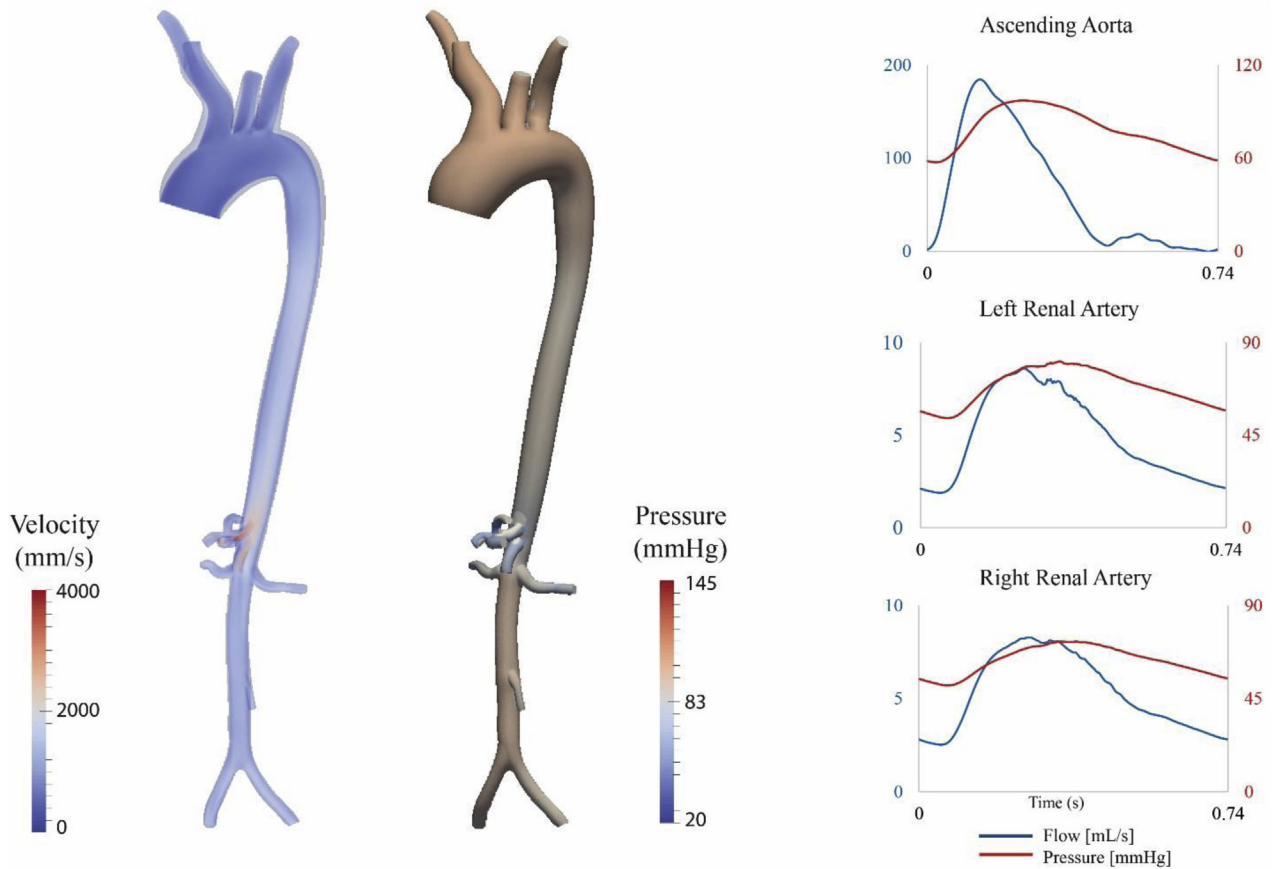
Supplementary Fig 3 (online only). *Left*, Three-dimensional maps of preoperative hemodynamics in peak systole. *Right*, Flow (*blue*) and pressure (*red*) waveforms in the ascending aorta, left renal artery, and right renal artery. The renal artery waveforms reveal nearly normal systole-dominated flows.

Supplementary Table I (online only). Simulated mean flow rates (mL/min)

Vessel	Preoperative model	Control
Left common carotid artery	28	28
Left subclavian artery	27	27
Right common carotid artery	28	28
Right subclavian artery	27	28
Superior mesenteric artery	57	56
Left gastric artery	29	28
Splenic artery	30	29
Hepatic artery	26	25
Left renal artery	29	30
Right renal artery	31	32
Inferior mesenteric artery	9	9
Left iliac artery	28	28
Right iliac artery	28	29

Hepatic left artery in preoperative model includes the addition of mean flow from both hepatic artery 1 and hepatic artery 2. Mean flows for all branches were matched within 5% error margins.

Supplementary Table II (online only). Parameter values for the three-element Windkessel models used in the preoperative model and all postoperative models

Vessel	Preoperative model			Postoperative model		
	Rp	C	Rd	Rp	C	Rd
Left common carotid artery	0.3401	6.580	1.9276	0.3401	6.580	1.0712
Left subclavian artery	0.3426	6.270	1.9523	0.3426	6.270	1.1043
Right common carotid artery	0.3402	6.580	1.9282	0.3402	6.580	1.0693
Right subclavian artery	0.3353	6.270	1.9103	0.3353	6.270	1.0833
Superior mesenteric artery	0.0236	5.367	0.3992	0.0236	5.367	0.5731
Left gastric artery	0.0152	1.568	0.2586	0.0152	1.568	0.2586
Splenic artery	0.0264	2.405	0.4457	0.0264	2.405	0.4457
Hepatic artery 1	0.0003	1.690	0.0051	0.0003	1.690	0.0051
Hepatic artery 2	0.0842	3.000	1.5033	0.0842	3.000	1.5033
Left renal artery	0.2090	3.537	0.8358	0.2090	3.537	0.8358
Right renal artery	0.2034	3.537	0.8136	0.2034	3.537	0.8136
Inferior mesenteric artery	0.2889	0.697	4.8701	0.2889	0.697	4.8701
Left iliac artery	0.1013	2.091	1.7557	0.1013	2.091	1.7557
Right iliac artery	0.0994	2.091	1.7313	0.0994	2.091	1.7313

C, Capacitor (mm^3 Pa^{-1}); *Rd*, distal resistor (Pa s mm^{-3}); *Rp*, proximal resistor (Pa s mm^{-3}).